

Journal of Solar Energy Research (JSER)

Journal homepage: www.jser.ut.ac.ir



Enhancing the Photovoltaic Performance of lead-free CH₃NH₃SnBr₃ Solar Cells via Compressive Strain Engineering: A Numerical Investigation

Fatima Zahra Znaki^{a*}, Khalid Said^a, Jihane Znaki^a, Mohamed Adadi^a, Hassane Moustabchir^a, Samir Chtita^b, Adil Touimi Benjelloun^c, Souad El khattabi^{a*}

^cLIMAS, Faculty of Sciences Dhar El Mahraz, Sidi Mohamed Ben Abdellah University, Fez, Morocco.

ARTICLE INFO

Article Type:

Research Article

Received:2025.06.05 Accepted in revised form:2025.10.11

Keywords:

Perovskite solar cell; CH₃NH₃SnBr₃; SCAPS-1D; Efficiency; Compressive strain

ABSTRACT

Perovskite solar cells have emerged as a promising alternative to conventional silicon photovoltaics. Despite this progress, challenges related to long-term stability persist, particularly those arising from the presence of lead. To address these issues, researchers are actively developing lead-free materials that can deliver comparable performance. In this study, we use SCAPS-1D numerical simulations to investigate the photovoltaic performance of hybrid organic-inorganic perovskite solar cells based on CH₃ NH₃ SnBr₃. Our analysis focuses on the influence of compressive strain on device performance. We investigated strain levels (0%, -2%, -4%, and -6%) and found that -6% strain yielded the best performance. Furthermore, we systematically examined the effects of absorber thickness, bulk defect density, interface defect density, and operating temperature. The optimized device under -6% strain delivered an open-circuit voltage of 1.16 V, a short-circuit current density of 31.60 mA/cm², a fill factor of 89.02%, and a theoretical power conversion efficiency of 32.82%. Moreover, the applied compressive strain enhances the structural stability, offering a novel route toward efficient and durable lead-free perovskite solar cells. These findings demonstrate that strain engineering is a promising strategy to enhance the performance of lead-free perovskite solar cells while remaining consistent with the fundamental efficiency limits of single-junction devices.

Cite this article: Znaki, F. Z., Said, K., Znaki, J., Adadi, M., Moustabchir, H., Chtita, S., Touimi Benjelloun, A. and El khattabi, S. (2025). Enhancing the Photovoltaic Performance of lead-free CH3NH3SnBr3 Solar Cells via Compressive Strain Engineering: A Numerical Investigation. Journal of Solar Energy Research, 10(3), 2475-2490. doi: 10.22059/jser.2025.396766.1580

DOI: 10.22059/jser.2025.396766.1580



©The Author(s). Publisher: University of Tehran Press.

^a Laboratory of Engineering, Systems and Applications, National School of Applied Sciences, Sidi Mohamed Ben Abdellah University, Fez, Morocco.

^b Laboratory of Physical Chemistry of Materials, Faculty of Sciences Ben M'Sik, Hassan II University of Casablanca, P.O. Box 7955, Casablanca, Morocco.

^{*}Corresponding Authors Email:fatimazahra.znaki@usmba.ac.ma and Souad.elkhattabi@usmba.ac.ma

1. Introduction

Fossil fuels, including coal, gas, and oil, were the predominant energy sources in many regions. However, since fossil fuels depleted the world's resources, produced pollutants, and contributed significantly to carbon emissions and climate change, it became necessary to search for cleaner alternatives. For this reason, many countries encouraged the use of renewable energy. Unlike conventional energy sources, renewable energy did not run out and was less polluting, making it a strong alternative. Among renewables, solar energy was the most abundant and had the lowest environmental impact, which made it a promising candidate [1] The fabrication of solar cells improved dramatically from one generation to another [2] Electricity was generated through the conversion of light into electrical energy using a solar cell device, a process known as the photovoltaic effect. Previous studies examined strategies to improve the efficiency and reliability of solar energy systems [3]. However, there was insufficient attention to important challenges related to material stability and long-term Jiwanapurkar degradation. and Bhargav [4] investigated TiO2 and ZnO nanofluids for beamsplitting photovoltaic-thermal systems, demonstrating enhanced spectral absorption. Similarly, Lalit Jyani et al.[5] examined sustainable cooling methods for PV panels in high-temperature regions, highlighting performance optimization strategies. These developments brought attention to the continued exploration of new materials and system designs to further enhance photovoltaic performance, which was the focus of the present

Perovskite materials were known for their high efficiency, flexibility, strong absorption of incident light, tunable bandgap, and low fabrication cost, which made them promising candidates for nextgeneration solar cells. Classified within the third generation of photovoltaics, also known as emerging technologies, their efficiency increased from 3% in organic-inorganic hybrid halide lead perovskites in 2009 [6] to over 33% in tandem perovskite/silicon devices, surpassing the maximum efficiency achieved by traditional mono- and polycrystalline silicon cells. Despite power conversion efficiencies exceeding 23% [7] organic-inorganic hybrid halide lead perovskites such as CH3 NH3 PbI3 faced challenges related to stability. The presence of lead rendered them unstable and toxic, which limited commercialization. Recent reviews highlighted both the rapid efficiency gains and the persistent

challenges of perovskite solar cells, especially concerning lead toxicity and long-term stability [8]. To address lead toxicity, researchers proposed substituting lead with elements possessing similar electronic properties. Tin (Sn), being in the same group of the periodic table, exhibited comparable characteristics and a similar ionic radius [9]. Several lead-free perovskite alternatives were explored, including hybrid organic-inorganic tin halide perovskites [10] [11] halide double perovskites [12], and germanium halide perovskites [13] [14]. In this study, we focused on a tin-based perovskite material in which lead was replaced by tin. In a hybrid organic-inorganic halide perovskite (ABX₃), A is an organic monovalent cation, in this case methylammonium (CH₃ NH₃); B is a divalent cation, here tin (Sn2+); and X is a halide anion, typically Cl, Br, or I (Figure 1).

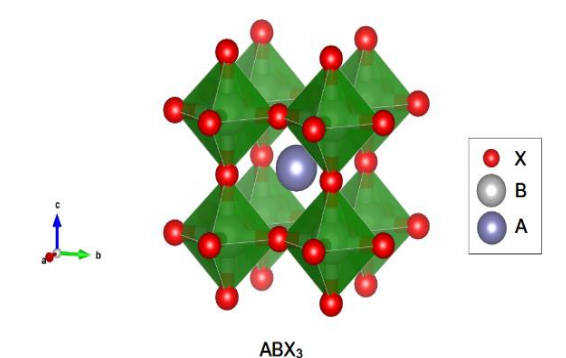


Figure 1. General Perovskite structure of the formula ABX₃

Tin-based hybrid perovskites exhibit notable stability [15], high charge-carrier mobility, and low binding energy; they contain a narrow optical bandgap and a high optical absorption coefficient [16, 17]. Despite being suitable materials for optoelectronic applications, CH₃ NH₃ SnBr₃ had a relatively wide experimental bandgap of 2.15 eV [18]. However, this value could be favourably reduced through several strategies, such as halide and cation engineering [19-21] or structural variation of the corner-sharing octahedral network, for example, by substituting the A-site cation with a larger ion. For engineering stable perovskites, Goldschmidt's tolerance factor [22] plays an

important role; it is defined as t =
$$\frac{\left(r_A + r_X\right)}{\sqrt{2\left(r_B + r_X\right)}}$$
,

where r_A, r_B, and r_X are the ionic radii of ions A, B, and X, respectively[23]. Doping, which involved the introduction of dopant materials into the charge-transport layers or the perovskite layer, was another

strategy used to enhance perovskite solar cell performance. This technique increased carrier mobility or shifted the Fermi level [24]. Another approach was mechanical strain [25] or high pressure[26, 27] [28], which extended the carrier lifetime and improved photovoltaic (PV) performance. Strain (ϵ) is the deformation of the crystal structure resulting from applied stress; it is

defined as
$$\varepsilon = \frac{a_0 - a}{a_0}$$
 where a_0 and a are the lattice

constants of strain-free and strained materials, respectively [29]. It is called tensile if the lattice increases in length under applied forces. In contrast, the strain is called compressive if the lattice decreases in length under stress [30]. Strain can modify the crystal structure of perovskites, directly influencing the bandgap. For example, compressive strain can reduce the bandgap, while tensile strain can increase it [31]. Strain can also affect the stability and performance of perovskite solar cells. Compressive strain can enhance the intrinsic stability of perovskites, while tensile strain can accelerate their degradation [32]. Overall, strain management is essential for optimizing the properties of perovskites, notably by adjusting the bandgap to improve the efficiency and stability of solar cells. Figure 2 presents the energy level diagram of the charge transport in a perovskite solar cell. It illustrates the choice of perovskite, electron transport, and hole transport materials, which are determined by the energy diagram.

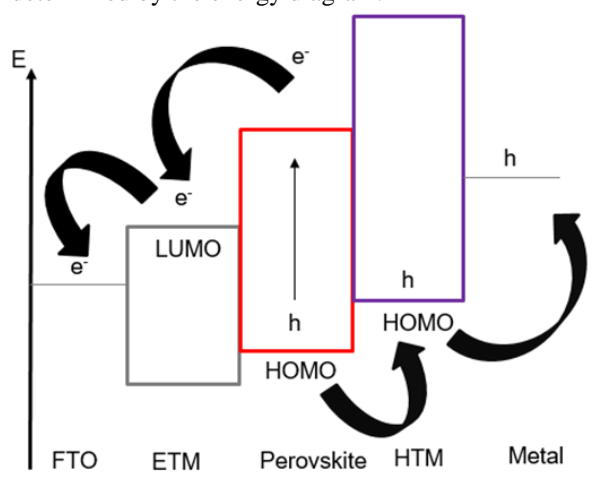


Figure 2. Energy level diagram

The HOMO energy of HTMs should ideally be higher than or similar to the valence band of the perovskite, while the LUMO energy of ETMs should be lower than or comparable to the

conduction band [33]. There was considerable interest in NiO as a hole transport material for perovskite solar cell applications [34]. NiO_x films are known for their high charge-extraction ability and low interfacial charge recombination [35] [36]. SnO₂ is also recognized as a promising electron transport material, with an energetically favourable conduction band and a wide bandgap that enhances electron transport. Consequently, many studies demonstrated that SnO₂ nanoparticles were effective in achieving highly efficient perovskite solar cells [37] [38] [39] [40]. In the present study, we investigated a perovskite solar cell based on CH₃ NH₃ SnBr₃ as the absorber layer. We proposed a model structure simulated with SCAPS-1D software, in which NiO was used as the hole transport material, SnO₂ as the electron transport material, Au as the back contact, and FTO as the front contact glass, as shown in Figure 3. Although Sn-based perovskites had been studied in terms of synthesis, stability, and device performance, the influence of strain on their photovoltaic behaviour had not been thoroughly addressed. In this work, we systematically investigated the effect of compressive strain on CH3 NH3 SnBr3 -based perovskite solar cells using SCAPS-1D simulations. By analyzing how strain modified the bandgap, charge transport, and efficiency, this study provided new insights into strain engineering as a promising approach for optimizing the performance of Sn-based perovskite solar devices. While strain engineering had been explored in Pb-free halide perovskites [41], its role in Sn-based perovskites such as CH₃ NH₃ SnBr₃ remained less understood.

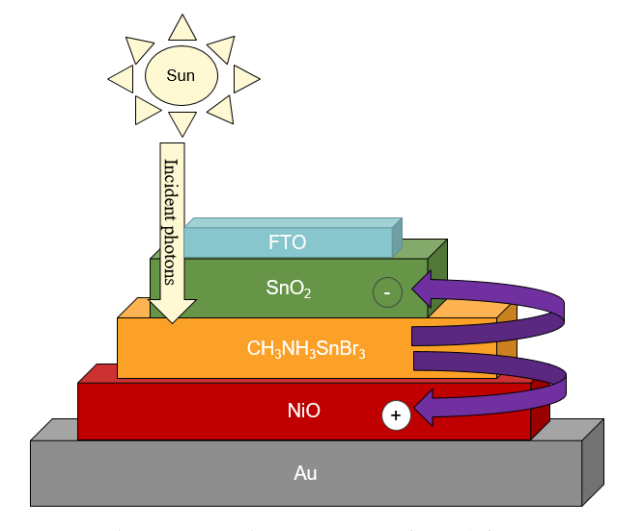


Figure 3. Device Structure of Lead-free CH₃NH₃SnBr₃-based solar cell

investigated the impact of applied compressive strain (-6%, -4%, -2%, and 0%) on the photovoltaic parameters the FTO/SnO₂ /CH₃ NH₃ SnBr₃ /NiO/Au solar device. Our findings showed that applying compressive strain significantly enhanced the photovoltaic performance of CH₃ NH₃ SnBr₃ -based perovskite solar cells by modifying key material properties. Compressive strain reduced the bandgap, enabled better light absorption, and increased photocurrent generation. In addition, it improved charge-carrier mobility and lifetime, which reduced energy losses and boosted overall efficiency. Understanding these mechanisms through modelling tools such as SCAPS-1D is essential for optimizing application of compressive strain in practical device fabrication. Although several studies have focused on improving the efficiency of lead-free perovskite solar cells, the issue of intrinsic instability remains a major challenge. In this work, we propose a novel approach based on compressive strain engineering to simultaneously enhance both the photovoltaic performance and structural stability CH₃ NH₃ SnBr₃ perovskite solar cells. To our knowledge, this is among the first numerical investigations exploring the dual impact of strain on efficiency and stability in Sn-based perovskites.

2. Device Architecture and Simulation Parameters

Simulation methods offer valuable tools for validating proposed physical models and intuitively examining individual device parameters to identify optimal performance conditions. Open-source software such as GPVDM, wxAMPS, SCAPS-1D, PC-1D, and AMPS-1D, along with commercial options including TCAD, COMSOL, and SILVACO ATLAS, are widely used in photovoltaic research. Among these, SCAPS-1D [42, 43] stands out for its ability to solve the fundamental semiconductor equations, including the Poisson equation and the continuity equations for electrons and holes. (Eqs. (1)- (3)). [44-46]

Poisson Equation:

$$\frac{d}{dx}(-\varepsilon(x)\frac{d\Psi}{dx}) = q[p(x) - n(x) + N_D^+(x) + N_A^-(x) + p_t(x) + n_t(x)]$$
(1)

Continuity equation for electron:

$$\frac{dJ_n}{dx} = G - R \tag{2}$$

Continuity equation for the hole:

$$\frac{dJ_p}{dx} = G - R \tag{3}$$

Where Ψ is the electrostatic potential, q is the electric charge, ϵ is the permittivity, p(x) and n(x) are the concentrations of holes and electrons, donor-type charged impurities and are the concentrations of trapped holes and electrons, respectively, J_n and J_p are the current densities of electrons and holes, R is the recombination rate, and G is the generation rate. Parameters such as PCE, V_{oc} , J_{sc} , and FF are related to each other as follows:

$$FF = \frac{P_{max}}{P_{in}} = \frac{I_{max} \times V_{max}}{V_{oc} \times I_{sc}}$$
(4)

$$PCE = \frac{FF \times V_{oc} \times I_{sc}}{P_{in}}$$
 (5)

Where P_{max} is the maximum power achievable, and P_{in} is the input solar power (AM1.5G spectrum) [47] [48] [49] The initial input parameters include the thickness, bandgap (E_g), electron affinity, dielectric constant (ϵ_r), electron and hole mobilities (μ_e and μp , as defined in Equation (6)), the mobility determined from the effective mass (as in Equation (7)), conduction band density of states (N_c) and valence band density of states (N_v), acceptor density (N_A) and donor density (N_D), and defect density (as defined in Equation (8)). The electron and hole thermal velocities are kept unchanged. These parameters, compiled from previous theories and earlier studies, are used in the simulations, as summarized in Table 1[50] [51].

Table 1. Simulation parameters for different layers of

Parameters	FTO	SC [50, 51] SnO ₂	CH ₃ NH ₃	NiO
			$SnBr_3$	
Thickness	0.400	0.010	0.500	0.200
(µm)				
$E_g(eV)$	3.5	3.3	2	3.6
χ(eV)	4	4	4.17	1.8
3	9	9	10	11.7
N_c (cm ⁻³)	$2.2 \times$	$2.2 \times$	2.2×10^{18}	$2.5 \times$
	10^{18}	10^{17}		10^{20}
N_{v} (cm ⁻³)	$1.8 \times$	$2.2 \times$	1.8×10^{18}	$2.5 \times$
	10^{18}	10^{16}		10^{20}
$V_{th,e}$ (cm s ⁻¹)	10^{7}	10^{7}	10^{7}	10^{7}
$V_{th,h}$ (cm s ⁻¹)	10^{7}	10^{7}	10^{7}	10^{7}
$\mu_e(\text{cm}^2 \text{Vs}^-)$	2×10^{1}	2×10^{2}	1.6	2.8
μ_h (cm ² Vs ⁻¹)	1×10^{1}	8×10^{1}	1.6	2.8
N_D (cm ⁻³)	1×10^{19}	1×10^{19}	10^{15}	0
$N_A(cm^{-3})$	0	0	10^{18}	10^{20}
N_t (cm ⁻³)	10^{14}	10^{14}	10^{14}	10^{14}

Table 2 presents the input parameters of the material under different perovskite According to a previous study [52] based on density functional theory, the bandgap decreases from 2 eV to 1.4 eV. The bandgap of the material is determined from the band diagram along with the effective mass (as in Equation (7)) [53]. Electron affinity is kept constant at 4.17 eV, while the dielectric permittivity is reduced under strain. The conduction band density of states (DOS) and valence band DOS are calculated using Equation (10) [54]. Thermal velocities are maintained at 10⁷ cm/s, and electron and hole mobilities are obtained from Equation (9). Defect density and total defect density are also kept unchanged.[55].

Electron and hole mobility:

$$\mu_e = \mu_p = \frac{qD_{(e,p)}}{kT}$$
 (6)

Effective mass:

$$m^* = (\frac{h}{2\pi \frac{\partial^2 E}{\partial k^2}}) \tag{7}$$

Defect density:

$$N_t = \frac{1}{\tau \sigma \nu}.$$
 (8)

Electron and hole mobility from effective mass:

$$\mu = \frac{e\tau}{m^*} \tag{9}$$

Valence band DOS and conduction band DOS:

$$N_{c,v} = 2\left(\frac{2\pi m^* kT}{h^2}\right)^{\frac{3}{2}} \tag{10}$$

Table 2. Simulation parameters of CH₃NH₃SnBr₃ under different strains [52]

	illuci ulli	cicii straiii	3 [32]	
Parameters	0%	-2%	-4%	-6%
Thickness	0.5	0.5	0.5	0.5
(μm)				
$E_{g}\left(eV\right)$	2	1.8	1.6	1.4
χ(eV)	4.17	4.17	4.17	4.17
3	4.1	4.2	4.5	4.7
N_c (cm ⁻³)	$1.2 \times$	8×10^{18}	8×10^{18}	8×10^{18}
	10^{19}			
N_v (cm ⁻³)	1.6×	1.1×	1×10^{19}	1×10^{19}
	10^{19}	10^{19}		
$V_{th,e}$ (cm s ⁻¹)	10^{7}	10^{7}	10^{7}	10^{7}
$V_{th,h}$ (cm s ⁻¹)	10^{7}	10^{7}	10^{7}	10^{7}
$\mu_e(cm^2 Vs^{-1})$	1×10^{0}	1.3×10^{0}	1.3×10^{0}	1.3×10^{0}
μ_h (cm ² Vs ⁻¹)	1×10^{0}	1×10^{0}	1.1×10^{0}	1.1×10^{0}
N_D (cm ⁻³)	10^{15}	10^{15}	10^{15}	10^{15}
$N_A(cm^{-3})$	10^{18}	10^{18}	10^{18}	10^{18}
N_t (cm ⁻³)	10^{14}	10^{14}	10^{14}	10^{14}

In this study, we simulated the device based on CH₃ NH₃ SnBr₃ under different strains (0%, -2%, -4%, and -6%) according to a previous study [52]. The temperature is fixed at 300 K, and the illumination is set to 1000 W/m² at AM 1.5 G. The SnO₂ /CH₃ NH₃ SnBr₃ and CH₃ NH₃ SnBr₃ /NiO interface layers have neutral defect densities of 10^{12} cm⁻² and 10^{11} cm⁻², respectively. The initial calculated parameters using the theoretical values in Table 1 are as follows: $V_{oc} = 1.1119$ V, $J\Box_c = 32.0579$ mA/cm², FF = 85.14%, and PCE = 30.35%.

3. Results and Discussion

• Performance of the device under different strains

Before exploring the effects of varying parameters, Figure 4 presents the energy band diagram of the simulated $CH_3 NH_3 SnBr_3$ -based solar cell, showing SnO_2 as the electron transport layer (ETL) and NiO as the hole transport layer (HTL).

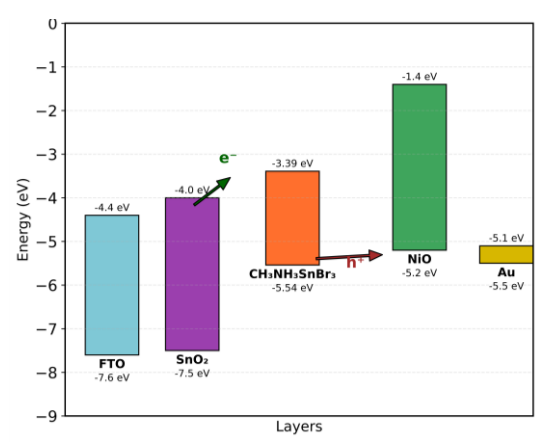


Figure 4. Schematic illustration of the charge transfer process in a lead-free device.

The device shows its best performance under a compressive strain of -6% applied CH₃ NH₃ SnBr₃ perovskite laver. Most photovoltaic parameters increase in value, except for the open-circuit voltage (V_{oc}) . Specifically, V_{oc} decreases from 1.93 V at 0% strain to 1.13 V at -6%. In contrast, the short-circuit current density (J_{sc}) rises from 11.81 mA/cm² to 28.66 mA/cm², while the fill factor (FF) improves from 69.66% to 88.42%. As a result, the power conversion efficiency (PCE) increases significantly from 15.89% to 28.86%, which represents a notable enhancement for photovoltaic applications. Figure 5 and Table 3 present the range of values obtained under different strain conditions. These results are consistent with those reported in the literature [56]. The strain levels examined here fall within the range achievable in experimental devices through techniques such as substrate-induced strain, lattice mismatch, mechanical bending of thin films. Previous studies have confirmed that moderate strain can be effectively applied in real devices, suggesting that the improvements predicted in this work could be realized in practical applications [57, 58].

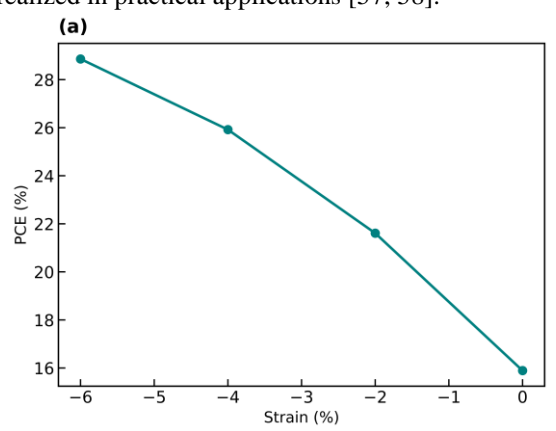


Figure 5a. Variation of Power Converion Efficiency with applied strain for CH₃ NH₃ SnBr₃ -based perovskite solar cells

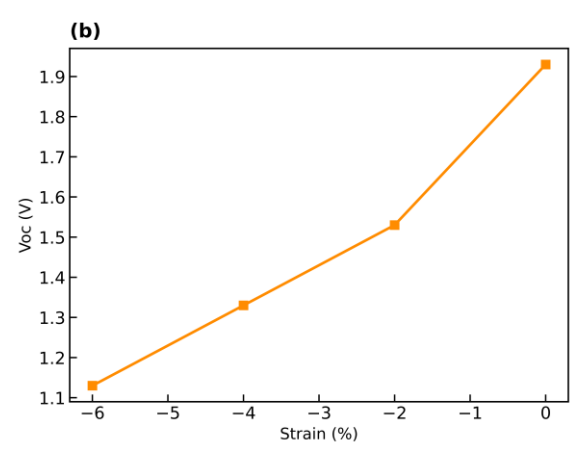


Figure 5b. Variation of V_{oc} with applied strain for CH₃ NH₃ SnBr₃ -based perovskite solar cells

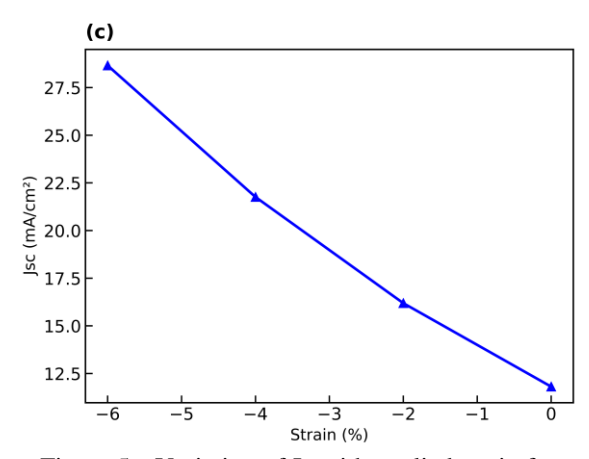


Figure 5c. Variation of J_{sc} with applied strain for $CH_3\ NH_3\ SnBr_3$ -based perovskite solar cells

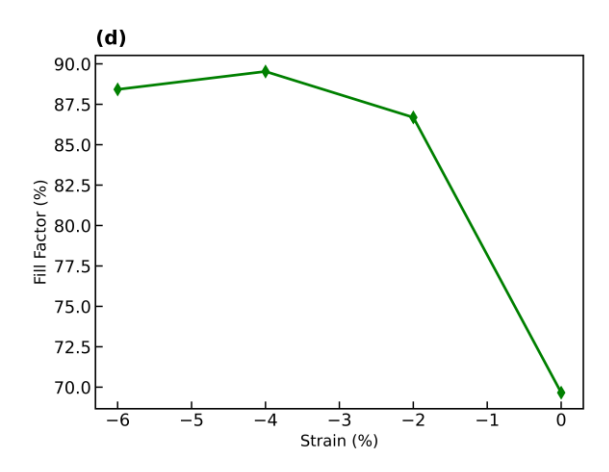


Figure 5d. Variation of Fill Factor with applied strain for CH₃ NH₃ SnBr₃ -based perovskite solar cells

Table 3. Photovoltaic performance of the device under different strains.

Strains	FF(%)	V _{oc} (V)	J _{sc} (mA cm ⁻²)	PCE(%)
0%	69.66	1.93	11.81	15.89
-2%	86.69	1.53	16.19	21.61
-4%	89.53	1.33	21.76	25.92
-6%	88.42	1.13	28.66	28.86

To investigate the effects of different parameters on the performance of our perovskite solar cell, we will simulate variations in the absorber layer thickness. We will also examine the influence of doping density in both the absorber layer and the ETL/HTL interfaces. In addition, the effects of operating temperature in the range of 300–400 K will be analyzed. All these parameters will be studied under different strain conditions, ranging from 0% to -6%, to provide a comprehensive evaluation of their impact on device efficiency.

• Thickness variation of the absorber layer

The simulation results revealed that increasing the absorber thickness from 0.1 µm to 1 µm led to significant improvements in all photovoltaic parameters, particularly the power conversion efficiency (PCE), which increased and then saturated as the thickness approached 1 µm due to enhanced light absorption and carrier generation. Applying compressive strain (-6% to 0%) further influenced the device performance. While PCE, short-circuit current density (Jsc), and fill factor (FF) improved with increasing compressive strain, reaching peak values under -6% strain, the open-circuit voltage (Voc) exhibited a decreasing trend. This suggested that strain enhanced carrier collection and transport, possibly by improving band alignment and reducing recombination losses, but it may also have introduced defect states or bandgap narrowing that limited Voc. Figure 6 presents the influence of absorber thickness variation on CH3NH3SnBr3based devices under different strains. Overall, the combination of optimized thickness and moderate compressive strain resulted in a notable performance enhancement, with PCE exceeding 30% under optimal conditions. The absorber layer played a pivotal role in perovskite solar cells by governing light absorption and charge carrier generation. Variations in absorber thickness typically altered the diffusion lengths and lifetimes of photogenerated holes and electrons. Based on these findings, we

selected 1.0 μm as the ideal thickness for further modelling.

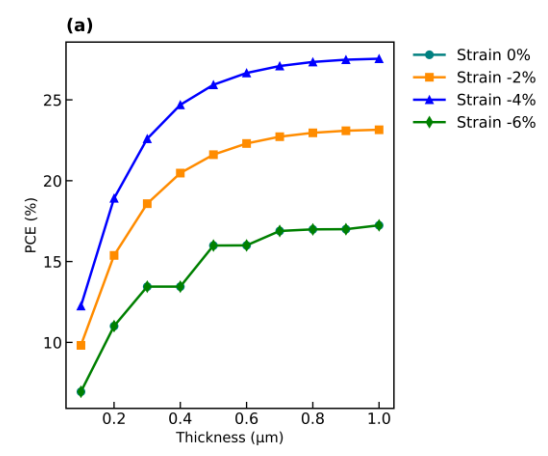


Figure 6a. Variation of Power conversion efficiency (PCE) with perovskite layer thickness under different strain conditions.

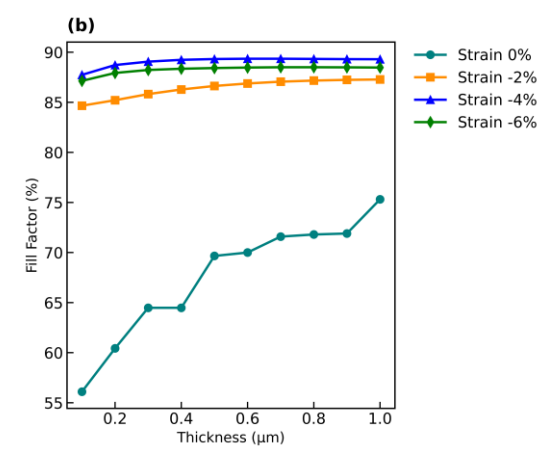


Figure 6b. Variation of Fill Factor with perovskite layer thickness under different strain conditions.

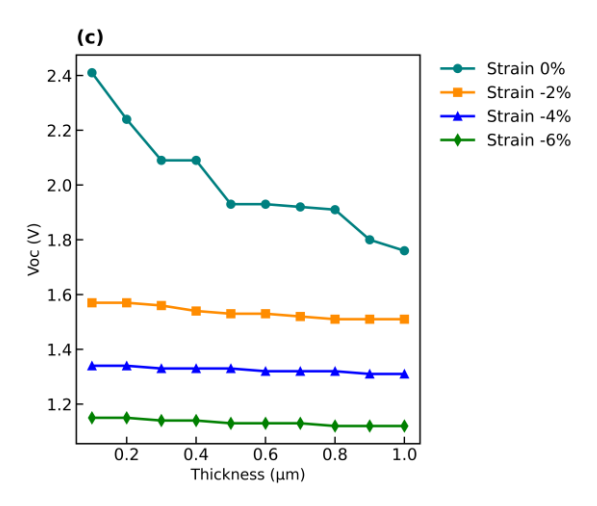


Figure 6c. Variation of V_{oc} with perovskite layer thickness under different strain conditions.

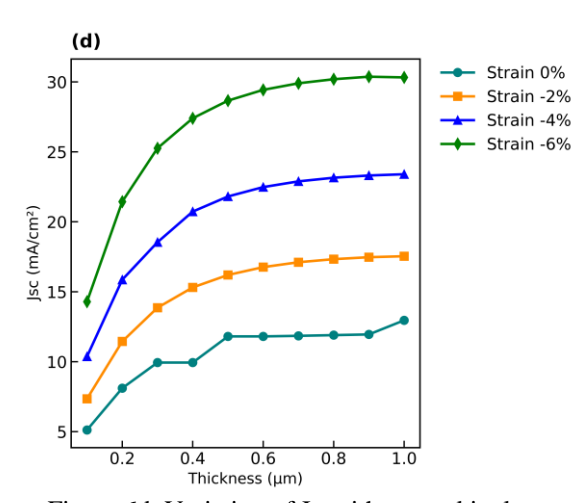


Figure 6d. Variation of J_{sc} with perovskite layer thickness under different strain conditions.

Variation in CH₃NH₃SnBr₃ Defect Density

Perovskite absorber layers often contained defects such as interstitials, vacancies, Frenkel defects, and Schottky defects. A high density of these defects significantly degraded device stability. The total defect density (NT) of the absorber layer (CH₃ NH₃ SnBr₃) was varied between 10¹² cm⁻³ and 10¹⁶ cm⁻³ to determine its effect on perovskite solar cell efficiency. Figure 7 illustrates the fluctuations of device parameters with changing N_T values. Doping density also significantly influenced device performance. As defect density increased, the open-circuit voltage (Voc) and fill factor (FF) decreased due to enhanced recombination, while the short-circuit current density (J_{sc}) decreased more strongly under compressive strain (-6%), suggesting that strain improved carrier transport or reduced recombination at lower defect levels. The power conversion efficiency (PCE) increased with strain at low defect densities but dropped at higher defect densities, indicating that while strain enhanced performance in relatively defect-free regions, excessive defects outweighed these benefits. Overall, defect density negatively impacted Voc, FF, and PCE, while Jsc exhibited an unexpected decrease at higher defect densities under strain. An increase in N_T within the perovskite absorber layer reduced overall device performance due to the proliferation of recombination pathways and trap states [59] Based on these findings, we selected a defect density of 1012 cm⁻³ as the optimal value for further simulations.

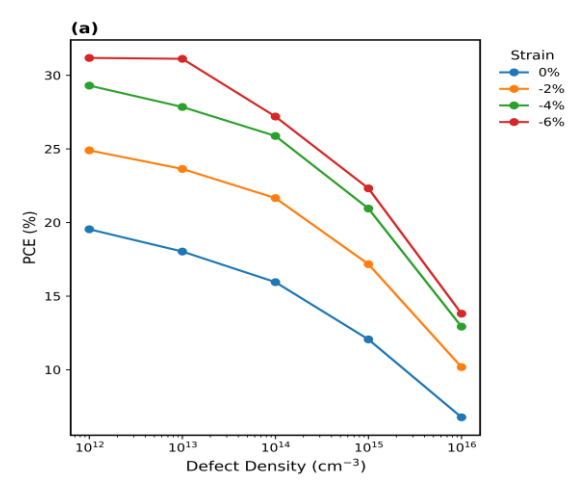


Figure 7a. Variation of Power Conversion Efficiency as a function of defect density under different biaxial strain levels (0%, -2%, -4%, and -6%).

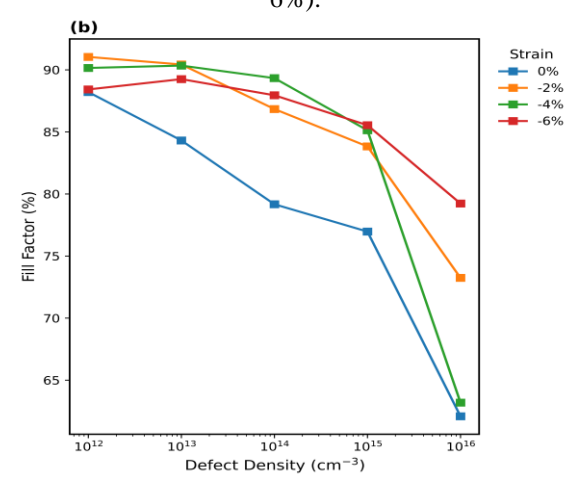


Figure 7b. Variation of Fill Factor as a function of defect density under different biaxial strain levels (0%, -2%, -4%, and -6%).

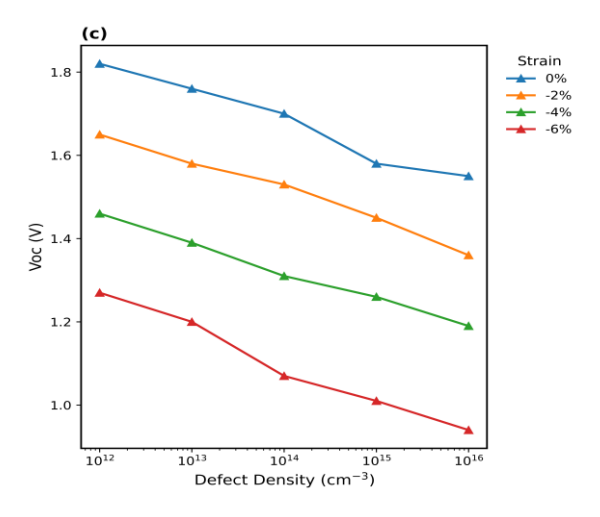


Figure 7c. Variation of V_{oc} as a function of defect density under different biaxial strain levels (0%, -2%, -4%, and -6%).

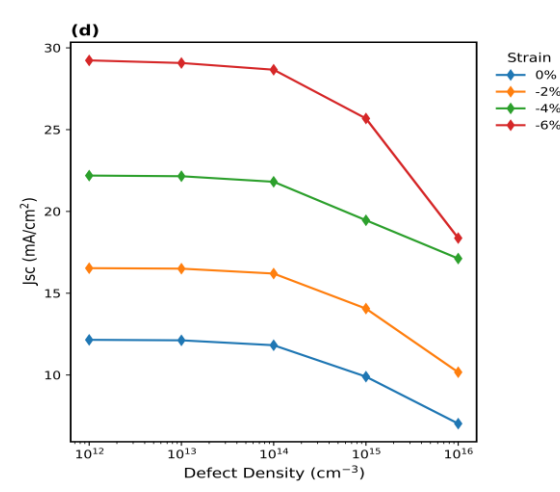


Figure 7d. Variation of short-circuit current density (Jsc) as a function of defect density under different biaxial strain levels (0%, -2%, -4%, and -6%)

Variation in SnO₂/CH₃NH₃SnBr₃ interface defect density

We incorporated interface defects into our baseline simulation to better replicate real-world conditions. The SnO₂ /CH₃ NH₃ SnBr₃ interface density significantly impacted both the efficiency and stability of the solar cell device. To investigate this effect, we simulated various defect densities at the SnO₂ /CH₃ NH₃ SnBr₃ interface, ranging from 10¹⁰ cm⁻³ to 10¹⁷ cm⁻³. The defect states were assumed to be uniformly distributed at the center of the SnO₂ /perovskite interface, meaning they were evenly spread across the boundary between the electron transport layer (ETL) and the absorber layer. Figure 8 illustrates the effect of varying interface defect density on device parameters. As defect density increased, the power conversion efficiency (PCE), open-circuit voltage (Voc), and fill factor (FF) all showed a clear decline, more pronounced at higher defect densities due to enhanced non-radiative recombination interface, except for the FF at 0%. The short-circuit current density (Jsc) remained nearly constant across all defect levels and strain values, indicating that carrier generation was not strongly influenced by interface defects in this configuration. Notably, higher compressive strain levels (-6%) consistently yielded superior PCE, FF, and Jsc across all defect densities, likely due to enhanced charge transport or improved band alignment. In contrast, the negative impact of interface defects was more pronounced at lower strain levels (particularly 0%). These trends highlighted the synergistic role of strain engineering in mitigating defect-induced performance degradation. Based on our findings, an ETL/perovskite defect density of 10^{10} cm⁻³ provided the optimal performance. Therefore, we adopted this value for subsequent simulations.

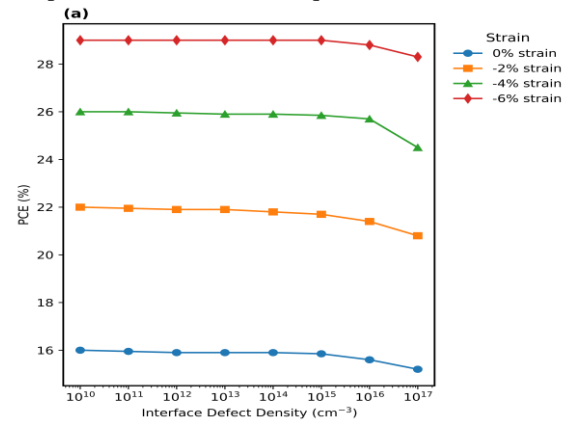


Figure 8a. Effect of interface defect density on the Pwer Conversion Efficiency of strained devices

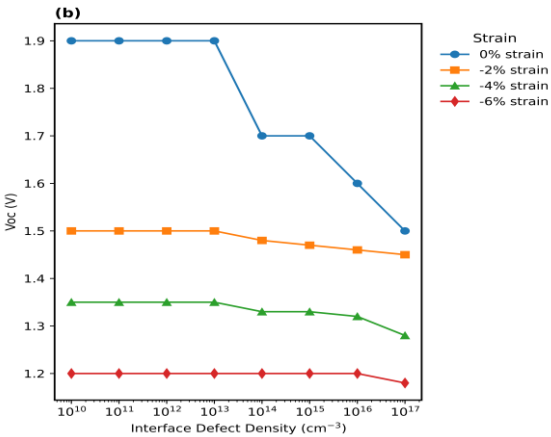


Figure 8b. Effect of interface defect density on the $V_{\rm oc}$ of strained devices

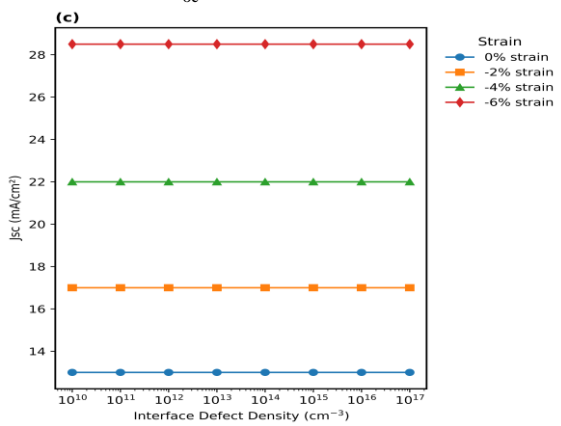


Figure c. Effect of interface defect density on the $J_{\rm sc}$ of strained devices

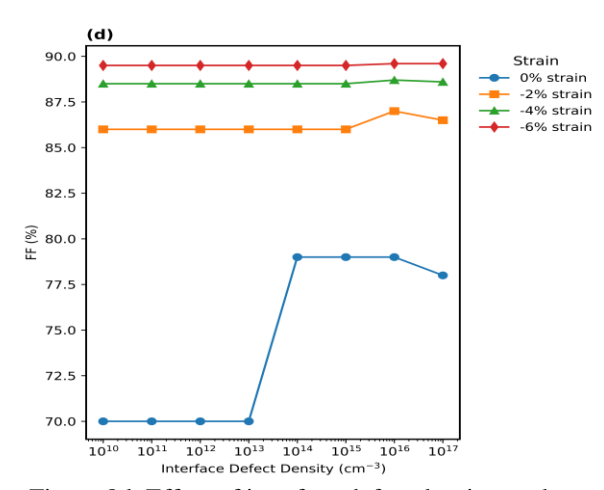


Figure 8d. Effect of interface defect density on the Fill Factor of strained devices

• Variation in CH₃NH₃SnBr₃/NiO interface defect density

To study the influence of interface defects on device performance, we intentionally increased their density in our simulations. The defect density at the CH₃ NH₃ SnBr₃ /NiO interface significantly influenced both the efficiency and stability of the solar cell. We simulated various defect densities at this interface, ranging from 10^{10} cm⁻³ to 10^{15} cm⁻³, assuming that the defect states were uniformly distributed the at center of the CH₃ NH₃ SnBr₃ /NiO interface. In other words, defects were evenly spread across the boundary between the hole transport layer (HTL, NiO) and the absorber layer. Figure 9 presents the effect of varying interface defect density on parameters. With increasing defect density, most device parameters exhibited a general decline, although the fill factor (FF) showed a slight improvement. For example, as defect density increased from 10¹⁰ to 10¹⁵ cm⁻³, the power conversion efficiency (PCE) dropped sharply under -6% strain, from 28.83% to 20.22%, indicating that higher defect densities severely impaired charge transport and increased recombination. The shortcircuit current density (J_{sc}) and open-circuit voltage (V_{oc}) followed similar trends, particularly under stronger strain conditions, reflecting recombination rates at the defective interface. Interestingly, FF remained relatively stable across most defect levels, with only a slight drop at the highest densities and strains. Overall, increasing interface defect density adversely affected PSC

performance by trapping, recombining, or scattering holes as they migrated from the perovskite absorber to the HTL. Based on our findings, a perovskite/HTL defect density of 10^{10} cm⁻³ provided the optimal performance. Therefore, we adopted this value for subsequent simulations.

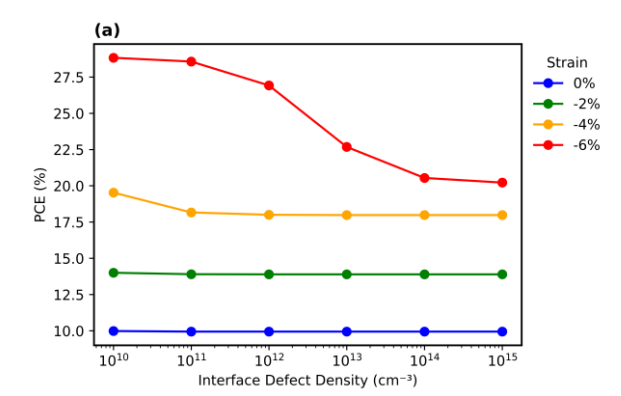


Figure 9a. Effect of interface defect density on the Power Conversion Efficiency of strained perovskite solar cells

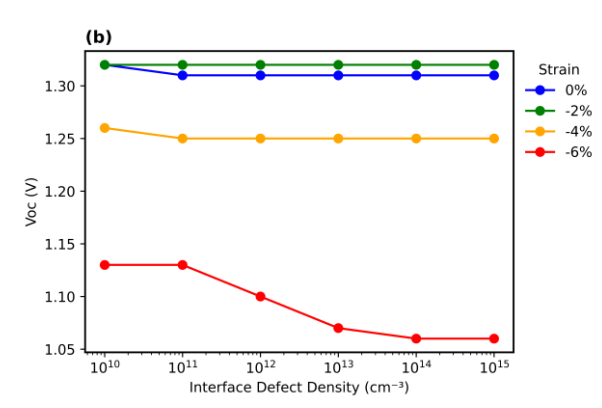


Figure 9b. Effect of interface defect density on the V_{oc} of strained perovskite solar cells

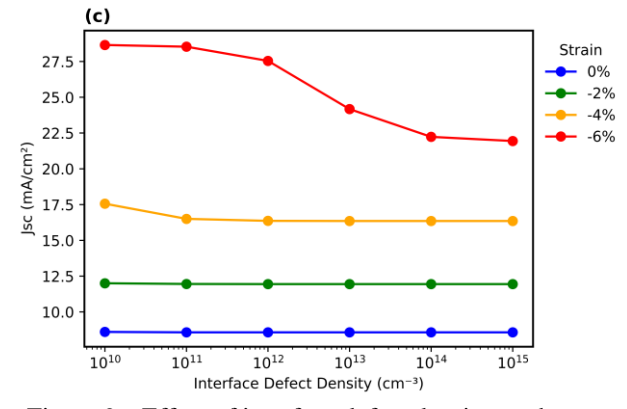


Figure 9c. Effect of interface defect density on the J_{sc} of strained perovskite solar cells

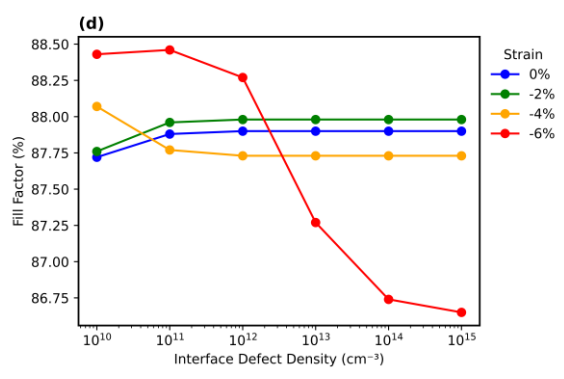


Figure 9d. Effect of interface defect density on the Fill Factor of strained perovskite solar cells

Variation in temperature

We examined the device's efficiency by varying the temperature from 300 K to 400 K. As shown in Figure 10, the perovskite solar cell parameters, including Voc, Jsc, FF, and PCE, varied with increasing temperature. At 0% strain, the PCE initially increased with temperature but then dropped slightly, mainly due to non-monotonic behaviour in V_{oc} and FF. These unusually high values may indicate unrealistic or error-prone results at low strain. As strain increased, the expected trends clearer: V_{oc} steadily declined temperature, likely due to enhanced recombination, while J_{sc} increased, possibly as a result of improved carrier mobility or enhanced light absorption. The fill factor decreased slightly with temperature under strain, consistent with increased series resistance or interface degradation. Overall, at higher compressive strain (especially -6%), the device demonstrated stronger thermal stability in terms of J_{sc} but suffered reductions in Voc and FF, leading to a gradual decline in PCE. An increase in temperature therefore decreased overall device performance due to higher recombination rates and an increased saturation current [60].

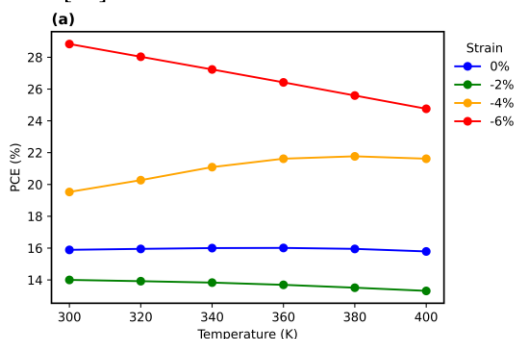


Figure 10a. Influence of temperature on the Power Conversion Efficiency of strained perovskite solar cells

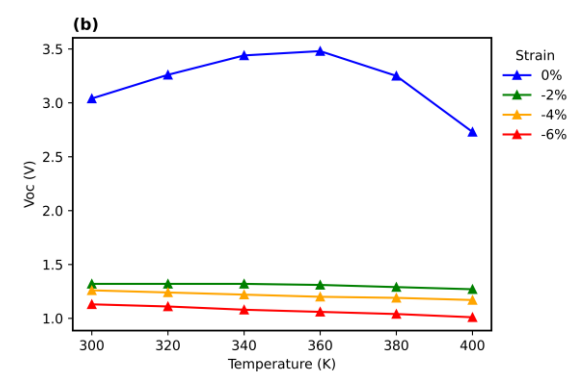


Figure 10b. Influence of temperature on the V_{oc} of strained perovskite solar cells

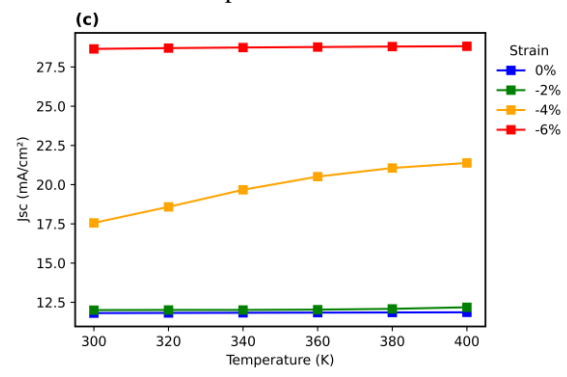


Figure 10c. Influence of temperature on the J_{sc} of strained perovskite solar cells

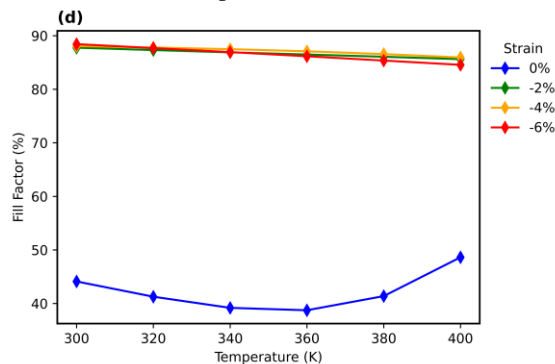


Figure 10d. Influence of temperature on the Fill Factor of strained perovskite solar cells

It is important to emphasize that all the results obtained in this study, including values for current density, open-circuit voltage, and efficiency, strictly adhered to the fundamental limits of single-junction solar cells. We ensured that the maximum values predicted did not exceed those attainable by a single absorber under the AM1.5 solar spectrum, as highlighted by Morales-Acevedo in his critical analysis of recent publications. By avoiding modelling errors and unrealistic extrapolations, this

study remained firmly grounded in the fundamentals of solar cell physics. [56].

• Best Performance of the Device

The optimized PSC performance was obtained with an absorber layer thickness of 1 μm , a defect density of 10^{12} cm $^{-3}$, an SnO $_2$ /perovskite interface defect density of 10^{10} cm $^{-3}$, and a perovskite/NiO interface defect density of 10^{10} cm $^{-3}$. Table 4 presents the optimal PSC efficiency under different strain conditions. The highest power conversion efficiency, achieved at -6% strain, was 32.82%, which exceeded the values reported in previous studies. This result is highly promising for the application of lead-free perovskites and further demonstrates the importance of strain engineering in enhancing the efficiency of perovskite-based devices.

Table 4. Photovoltaic parameters of the optimized structure under different strains

Strains	FF(%)	V _{oc} (V)	J _{sc} (mA cm ⁻²)	PCE(%)
0%	89.19	1.34	10.98	13.18
-2%	88.81	1.29	14.95	17.15
-4%	88.85	1.22	20.60	22.40
-6%	89.02	1.16	31.60	32.82

4. Conclusions

In this study, we modelled a regular n-i-p structured device with the perovskite layer CH₃ NH₃ SnBr₃ , varying absorber layer thickness, doping density, CH₃ NH₃ SnBr₃ /NiO interface defect density, SnO₂ /CH₃ NH₃ SnBr₃ interface defect density, and operating temperature. The photovoltaic parameters were extracted under 0%, -2%, -4%, and -6% compressive strain using the SCAPS-1D software. Under optimized conditions, an absorber thickness of 1 µm, absorber defect density of 1012 cm⁻³, SnO₂ /perovskite interface defect density of 1010 cm⁻³, and perovskite/NiO interface defect density of 10¹⁰ cm⁻³, the maximum efficiency reached 32.82% at -6% strain for the FTO/SnO2 /CH3 NH3 SnBr3 /NiO/Au leadfree structure (Voc = 1.16 V, Jsc = 31.60 mA/cm^2 , FF = 89.02%). In contrast, the same device at 0%strain exhibited a PCE of only 13.18% (Voc = 1.34 $V, Jsc = 10.98 \text{ mA/cm}^2, FF = 89.19\%$).

Our analysis showed that temperature strongly influences device performance, with efficiency parameters gradually declining as temperature increases, while perovskite thickness played a

relatively minor role. The device configuration was stable at 300 K, confirming favourable baseline operation.

The key novelty of this work lies in systematically demonstrating, for the first time, how compressive strain engineering can dramatically enhance the performance of lead-free CH₃ NH₃ SnBr₃ perovskite solar cells. Efficiencies as high as 32.82% were predicted, far exceeding those of unstrained devices, while remaining within experimentally achievable strain ranges. These findings suggest that strain engineering can serve as an effective design parameter for advancing next-generation, lead-free perovskite photovoltaics.

This study was limited to theoretical modelling, and the predicted enhancements may differ in practice due to defects, interface effects, or strain relaxation during fabrication. Future research should therefore focus on experimental validation of strain engineering strategies, optimization of deposition techniques to achieve stable strain, and assessment of their impact on long-term stability and scalability. Beyond performance enhancement, our results reveal that compressive strain can improve the structural stability of CH₃ NH₃ SnBr₃ by reducing defect densities and suppressing nonradiative recombination pathways. This dual improvement in efficiency and stability highlights the novelty and potential of strain engineering for future lead-free perovskite solar cell designs. Importantly, all results in this work respect the physical limits of singlejunction devices, as outlined by Morales-Acevedo, ensuring the scientific credibility of our results.

Acknowledgments

This work was carried out with the support of the National Center for Scientific and Technical Research (CNRST) as part of the 'PhD-Associate Scholarship-PASS Program.

The authors acknowledge Dr. Marc Bergelman (University of Gent, Belgium) for providing SCAPS software.

Nomenclature	
AMPS-1D	Analysis of Microelectronic and Photonic Structures – 1
AMFS-1D	Dimensional
χ	Electron affinity (eV)
ε	Dielectric constant
ETM	Electron Transport Material

FF	Fill Factor
FTO	Fluorine-doped Tin Oxide
GPVDM	General Purpose Photovoltaic Device Model
НОМО	Highest Occupied Molecular Orbital
HTM	Hole Transport Material
Isc	Short-Circuit Current (mA/cm²)
Jn	Electron current density
Jp	Hole current density
LUMO	Lowest Unoccupied Molecular Orbital
μе	Electron mobility (cm ² V ⁻¹ s ⁻¹)
μh	Hole mobility (cm ² V ⁻¹ s ⁻¹)
NA	Acceptor concentration (cm ⁻³)
Nc	Effective Density of States in the Conduction Band (cm ⁻³)
ND	Donor concentration (cm ⁻³)
Nt	Trap density (cm ⁻³)
Nv	Effective Density of States in the Valence Band (cm ⁻³)
PCE	Power Conversion Efficiency
PC-1D	Personal Computer One- Dimensional
SCAPS-1D	Solar Cell Capacitance Simulator – 1 Dimensional
TCAD	Technology Computer-Aided Design
Voc	Open-circuit voltage (V)
Vth,e	Thermal velocity of electrons (cm s ⁻¹)
Vth,h	Thermal velocity of holes (cm s ⁻¹)
wxAMPS	Windows Extended Analysis of Microelectronic and Photonic Structures

References

- [1] Mohtasham, J. (2015). Review Article-Renewable Energies. The International Conference on Technologies and Materials for Renewable Energy, Environment and Sustainability –TMREES15, 74(1289-1297. https://doi.org/10.1016/j.egypro.2015.07.77
- [2] Sharma, S., K.K. Jain, and A. Sharma. (2015). Solar Cells: In Research and

- Applications—A Review. Materials Sciences and Applications, 06(12), 1145. https://doi.org/10.4236/msa.2015.612113
- [3] Seifpanah Sowmehsaraee, M., M. Ranjbar, and M. Abedi. (2022). Investigating the effect of nano-structured magnetic particles lanthanum strontium manganite on perovskite solar cells. Journal of Solar Energy Research, 7(1), 945-956. https://doi.org/10.22059/jser.2021.325062.1 205
- [4] Jiwanapurkar, P.R. and H.A. Bhargav. (2025). Spectroscopic Analysis of Water-Based TiO2 and ZnO Nanofluid for Fluid-Based Beam Split Photovoltaic-thermal System. Journal of Solar Energy Research, 10(Emerging Trends in Photothermal Conversion for Solar Energy Harvesting), 45-55.
 - https://doi.org/10.22059/jser.2025.379717.1 445
- [5] Jyani, L., et al. (2025). Sustainable Cooling Technique for Maximizing Performance of Photovoltaic Panel in The Hot Climate of Rajasthan. Journal of Solar Energy Research, 10(Emerging Trends in Photothermal Conversion for Solar Energy Harvesting), 56-71. https://doi.org/10.22059/jser.2025.389945.1 524
- [6] Kojima, A., et al. (2009). Organometal Halide Perovskites as Visible-Light Sensitizers for Photovoltaic Cells. Journal of the American Chemical Society, 131(17), 6050-6051. https://doi.org/10.1021/ja809598r
- [7] Yi, Z., et al. (2019). Will organic–inorganic hybrid halide lead perovskites be eliminated from optoelectronic applications? Nanoscale Advances, 1(4), 1276-1289. https://doi.org/10.1039/C8NA00416A
- [8] Sanga, L., et al. (2025). A review on perovskite materials for photovoltaic applications. Next Materials, 7(100494. https://doi.org/10.1016/j.nxmate.2025.1004
- [9] Ke, W., C.C. Stoumpos, and M.G. Kanatzidis. (2019). "Unleaded" Perovskites: Status Quo and Future Prospects of Tin Based Perovskite Solar Cells. Advanced Materials, 31(47), 1803230. https://doi.org/10.1002/adma.201803230

- [10] Hao, F., et al. (2014). Lead-Free Solid-State Organic-Inorganic Halide Perovskite Solar Cells. Nature Photonics, 8(489-494. https://doi.org/10.1038/nphoton.2014.82
- [11] Hardy, J., H. Fiedler, and J. Kennedy. (2025). A review on the current status and chemistry of tin halide perovskite films for photovoltaics. Progress in Materials Science, 101446. https://doi.org/10.1016/j.pmatsci.2025.1014
- [12] Zhou, X., et al. (2018). Recent theoretical progress in the development of perovskite photovoltaic materials. Journal of energy chemistry, 27(3), 637-649. https://doi.org/10.1016/j.jechem.2017.10.01
- [13] Krishnamoorthy, T., et al. (2015). Lead-free germanium iodide perovskite materials for photovoltaic applications. Journal of Materials Chemistry A, 3(47), 23829-23832.
 - https://doi.org/10.1039/C5TA05741H
- [14] Bisht, N., et al. (2025). Comparative performance simulation study of Germanium-based perovskite solar cells using SCAPS-1D. Materials Chemistry and Physics, 345(131241. https://doi.org/10.1016/j.matchemphys.202 5.131241
- [15] Raoui, Y., et al. (2021). Harnessing the potential of lead-free Sn–Ge based perovskite solar cells by unlocking the recombination channels. Sustainable Energy & Fuels, 5(18), 4661-4667. https://doi.org/10.1039/D1SE00687H
- [16] Bernal, C. and K. Yang. (2014). First-Principles Hybrid Functional Study of the Organic–Inorganic Perovskites CH ₃ NH ₃ SnBr ₃ NH ₃ NH ₃ NH ₃ The Journal of Physical Chemistry C, 118(42), 24383-24388. https://doi.org/10.1021/jp509358f
- [17] Yang, W.F., et al. (2020). Tin Halide Perovskites: Progress and Challenges. Advanced Energy Materials, 10(13), 1902584. https://doi.org/10.1002/aenm.201902584
- [18] Chiarella, F., et al. (2008). Combined experimental and theoretical investigation of optical, structural, and electronic properties of C H 3 N H 3 Sn X 3 thin films

- (X = Cl , Br). Physical Review B, 77(4), 045129. https://doi.org/10.1103/PhysRevB.77.0451
- [19] Amat, A., et al. (2014). Cation-Induced Band-Gap Tuning in Organohalide Perovskites: Interplay of Spin-Orbit Coupling and Octahedra Tilting. Nano Letters, 14(6), 3608-3616. https://doi.org/10.1021/nl5012992
- [20] Li, Y., et al. (2021). Bandgap tuning strategy by cations and halide ions of lead halide perovskites learned from machine learning. RSC advances, 11(26), 15688-15694.https://doi.org/10.1039/D1RA03117
- [21] Borriello, I., G. Cantele, and D. Ninno. (2008). <i>Ab initio</i> investigation of hybrid organic-inorganic perovskites based on tin halides. Physical Review B, 77(23), 235214. https://doi.org/10.1103/PhysRevB.77.2352
- [22] Goldschmidt, V.M. (1926). The laws of crystal chemistry. Naturwissenschaften, 14(21), 477-485. https://doi.org/10.1007/BF01507527
- [23] Goldschmidt, V.M. (1926). Die Gesetze der Krystallochemie. Die Naturwissenschaften, 14(21), 477-485. https://doi.org/10.1007/BF01507527
- [24] Ibrahim, et al. (2024). Emerging trends in low band gap perovskite solar cells: materials, device architectures, and performance optimization. Molecular Physics, e2316273. https://doi.org/10.1080/00268976.2024.231 6273
- [25] Cheng, S., et al. (2025). Enhanced electrical performance of perovskite solar cells via strain engineering. Energy & Environmental Science, 18(5), 2452-2461. https://doi.org/10.1039/D4EE03760J
- [26] Coduri, M., et al. (2019). Band Gap Engineering in MASnBr ₃ and CsSnBr ₃ Perovskites: Mechanistic Insights through the Application of Pressure. The Journal of Physical Chemistry Letters, 10(23), 7398-7405.
- https://doi.org/10.1021/acs.jpclett.9b03046
 [27] Basavarajappa, M.G., M.K. Nazeeruddin, and S. Chakraborty. (2021). Evolution of hybrid organic—inorganic perovskite

- materials under external pressure. Applied Physics Reviews, 8(4), https://doi.org/10.1063/5.0053128
- [28] Jiao, Y., et al. (2021). Strain Engineering of Metal Halide Perovskites on Coupling Anisotropic Behaviors. Advanced Functional Materials, 31(4), 2006243. https://doi.org/10.1002/adfm.202006243
- [29] Som, N.N., et al. (2018). Strain and layer modulated electronic and optical properties of low dimensional perovskite methylammonium lead iodide: Implications to solar cells. Solar Energy, 173(1315-1322.
 - https://doi.org/10.1016/j.solener.2018.06.05
- [30] Yu, H., et al. (2021). Is the strain responsible to instability of inorganic perovskites and their photovoltaic devices? Materials Today Energy, 19(100601. https://doi.org/10.1016/j.mtener.2020.1006 01
- [31] Yang, B., et al. (2022). Strain effects on halide perovskite solar cells. Chemical Society Reviews, 51(17), 7509-7530. https://doi.org/10.1039/D2CS00278G
- [32] Wu, J., et al. (2021). Strain in perovskite solar cells: origins, impacts and regulation. National science review, 8(8), nwab047. https://doi.org/10.1093/nsr/nwab047
- [33] Roy, P., et al. (2020). A review on perovskite solar cells: Evolution of architecture, fabrication techniques, commercialization issues and status. Solar Energy, 198(665-688. https://doi.org/10.1016/j.solener.2020.01.08
- [34] Li, Y., et al. (2023). High Fill Factor and Reduced Hysteresis Perovskite Solar Cells Using Small-Molecule-Engineered Nickel Oxide as the Hole Transport Layer. ACS Applied Energy Materials, 6(3), 1555-1564. https://doi.org/10.1021/acsaem.2c03434
- [35] Nkele, A.C., et al. (2020). The use of nickel oxide as a hole transport material in perovskite solar cell configuration: Achieving a high performance and stable device. International Journal of Energy Research, 44(13), 9839-9863. https://doi.org/10.1002/er.5563
- [36] Kuo, D.-W. and C.-T. Chen. (2025). A Dual Layer of NiO_{<i>x</i>} Hole-Transporting Material Boosting the Efficiency of Inverted Perovskite Solar

- Cells up to 20.7%. ACS Applied Energy Materials, 8(8), 5309-5316. https://doi.org/10.1021/acsaem.5c00312
- [37] Chen, Y., et al. (2019). SnO2-based electron transporting layer materials for perovskite solar cells: A review of recent progress. Journal of Energy Chemistry, 35(144-167. https://doi.org/10.1016/j.jechem.2018.11.01
- [38] Mao, G.-P., et al. (2018). Research progress in electron transport layer in perovskite solar cells. Rare Metals, 37(2), 95-106. https://doi.org/10.1007/s12598-017-0951-4
- [39] Jiang, Q., et al. (2017). Planar-Structure Perovskite Solar Cells with Efficiency beyond 21%. Advanced Materials, 29(46), 1703852. https://doi.org/10.1002/adma.201703852
- [40] Jiang, Q., et al. (2019). Surface passivation of perovskite film for efficient solar cells. Nature Photonics, 13(7), 460-466. https://doi.org/10.1038/s41566-019-0398-2
- [41] Said, K., et al. (2025). Coupled effects of strain and halogen substitution on the structural, optoelectronic, and photovoltaic characteristics of Pb-Free Cs2AgInBr6: Density functional theory approach using HSE, BSE, and numerical methods. Solar Energy, 299(113782. https://doi.org/10.1016/j.solener.2025.1137
- [42] Anwar, F., et al. (2017). Effect of Different HTM Layers and Electrical Parameters on ZnO Nanorod-Based Lead-Free Perovskite Solar Cell for High-Efficiency Performance. International Journal of Photoenergy, 2017(1-9. https://doi.org/10.1155/2017/9846310
- [43] Khadka, D.B., et al. (2018). Degradation of encapsulated perovskite solar cells driven by deep trap states and interfacial deterioration. Journal of Materials C, 6(1), Chemistry 162-170. https://doi.org/10.1039/C7TC03733C
- [44] Zyoud, S.H., et al. (2021). Numerical modeling of high conversion efficiency FTO/ZnO/CdS/CZTS/MO thin film-based solar cells: Using SCAPS-1D software. Crystals, 11(12), 1468. https://doi.org/10.3390/cryst11121468
- [45] Zhang, Y., et al. (2023). SCAPS simulation and DFT study of lead-free perovskite solar cells based on CsGeI3. Materials Chemistry

- and Physics, 306(128084. https://doi.org/10.1016/j.matchemphys.202 3.128084
- [46] Slami, A., M. Bouchaour, and L. Merad. (2019). Numerical study of based perovskite solar cells by SCAPS-1D. Int. J. Energy Environ, 3(17-21.
- [47] Ravidas, B.K., M.K. Roy, and D.P. Samajdar. (2023). Investigation of photovoltaic performance of lead-free CsSnI3-based perovskite solar cell with different hole transport layers: First Principle Calculations and SCAPS-1D Analysis. Solar Energy, 249(163-173. https://doi.org/10.1016/j.solener.2022.11.02
- [48] Haidari, G. (2019). Comparative 1D optoelectrical simulation of the perovskite solar cell. AIP Advances, 9(8), https://doi.org/10.1063/1.5110495
- [49] Lin, P., et al. (2014). Numerical simulation of Cu2ZnSnS4 based solar cells with In2S3 buffer layers by SCAPS-1D. Journal of Applied Science and Engineering, 17(4), 383-390.
 - https://doi.org/10.6180/jase.2014.17.4.05
- [50] Haneef, M., et al. (2024). Optimizing Leadfree MASnBr ₃ Perovskite Solar Cells for High-Efficiency and Long-Term Stability Using Graphene and Advanced Interface Layers. ACS Omega, 9(6), 7053-7060. https://doi.org/10.1021/acsomega.3c08981
- [51] Mushtaq, S., et al. (2023). Performance optimization of lead-free MASnBr3 based perovskite solar cells by SCAPS-1D device simulation. Solar Energy, 249(401-413. https://doi.org/10.1016/j.solener.2022.11.05
- [52] Said, K. and S. Elkhattabi. (2024). Structural, electronic, and optical study of lead-free perovskite CH3NH3SnBr3 under compressive strain using DFT and DFT+ U. Materials Science in Semiconductor Processing, 174(108242. https://doi.org/10.1016/j.mssp.2024.108242
- [53] Saidani, O., et al. (2024). Revealing the secrets of high performance lead-free CsSnCl3 based perovskite solar cell: A dive into DFT and SCAPS-1D numerical insights. Solar Energy Materials and Solar Cells, 277(113122. https://doi.org/10.1016/j.solmat.2024.11312

- [54] Ritu, et al. (2024). Selection of hole transport layers through lattice mismatching using SCAPS-1D. Optical and Quantum Electronics, 56(12), 1942. https://doi.org/10.1007/s11082-024-07447-8
- [55] Chauhan, A. and A. Oudhia. (2024).

 First Principle Density Functional
 Theory Derived Nonleaded KSn <sub>
 1- <i>×</i> </sub> Ge _{<i>×</i>} I ₃ Based Perovskite
 Solar Cells: A Theoretical Study. Energy
 Technology, 12(2), 2300772.
 https://doi.org/10.1002/ente.202300772
- [56] Morales-Acevedo, A. (2023). Fundamentals of solar cell physics revisited: Common pitfalls when reporting calculated and measured photocurrent density, open-circuit voltage, and efficiency of solar cells. Solar Energy, 262(111774. https://doi.org/10.1016/j.solener.2023.05.05
- [57] Sánchez-Pérez, M., et al. (2021). Substrate-induced strain effect on structural and magnetic properties of La0. 5Sr0. 5CoO3 films. Nanomaterials, 11(3), 781. https://doi.org/10.3390/nano11030781
- [58] Margariti, E., et al. (2025). Strain-induced modifications of thin film silicon membranes through physical bending. Materials, 18(10), 2335. https://doi.org/10.3390/ma18102335
- [59] Johnston, M.B. and L.M. Herz. (2016). Hybrid Perovskites for Photovoltaics: Charge-Carrier Recombination, Diffusion, and Radiative Efficiencies. Accounts of Chemical Research, 49(1), 146-154. https://doi.org/10.1021/acs.accounts.5b004
- [60] Ahmed, S., et al. (2021). Numerical development of eco-friendly Cs2TiBr6 based perovskite solar cell with allinorganic charge transport materials via SCAPS-1D. Optik, 225(165765. https://doi.org/10.1016/j.ijleo.2020.165765